arXiv:1004.4762v2 [hep-ph] 23 Jul 2010

# Effects of invisible particle emission on global inclusive variables at hadron colliders

**Andreas Papaefstathiou and Bryan Webber**

*Cavendish Laboratory, University of Cambridge,*
*J.J. Thomson Avenue, Cambridge, CB3 0HE, U.K.*
*Email:* `andreas@hep.phy.cam.ac.uk`, `webber@hep.phy.cam.ac.uk`

ABSTRACT: We examine the effects of invisible particle emission in conjunction with QCD initial state radiation (ISR) on quantities designed to probe the mass scale of new physics at hadron colliders, which involve longitudinal as well as transverse final-state momenta. This is an extension of our previous treatment [1] of the effects of ISR on global inclusive variables. We present resummed results on the visible invariant mass distribution and compare them to parton-level Monte Carlo results for top quark and gluino pair-production at the LHC. There is good agreement as long as the visible pseudorapidity interval is large enough ($\eta_{\max} \gtrsim 3$). The effect of invisible particle emission is small in the case of top pair production but substantial for gluino pair production. This is due mainly to the larger mass of the intermediate particles in gluino decay (squarks rather than W-bosons). We also show Monte Carlo modelling of the effects of hadronization and the underlying event. The effect of the underlying event is large but may be approximately universal.

KEYWORDS: Hadronic Colliders, QCD Phenomenology, Supersymmetry Phenomenology, Beyond Standard Model.

# Contents

## 1. Introduction

Amongst the many observables that could be of use in the search for new physics at hadron colliders, those that do not depend on detailed hypotheses about the structure of the final state may be the most suitable for an initial general survey of the high-energy frontier. Quantities of this type have been investigated and named *global inclusive* observables in ref. [2]. Such quantities can provide information on the energy scales of new hard processes, for example the production of exotic heavy particles, without imposing prejudices about the nature of the new dynamics.

One may distinguish between global inclusive observables that depend only on transverse momenta, such as the visible and missing transverse energies, and observables such as the visible energy and invariant mass, which depend also on longitudinal momenta. The former are not affected by the unknown motion of the hard process in

the collider frame, in the approximation that the process is initiated by partons moving collinearly with the beams. However, the colour charges of those partons and the high scale of the hard process necessarily imply that there is significant initial-state QCD radiation (ISR), which contributes to both types of global inclusive observables.

In ref. [2] various global inclusive observables were investigated, including those that make use of longitudinal as well as transverse momentum components. The quantities studied included the visible energy $E$, i.e. the sum of energies of particles registered by the detector, and the visible invariant mass $M$,

$$M = \sqrt{E^2 - P_z^2 - \not{E}_T^2} \,, \tag{1.1}$$

where $P_z$ is the visible longitudinal momentum. Here $\not{E}_T$, the missing transverse energy, is in practice defined as the negative of the total visible transverse momentum, so that (1.1) does indeed define a Lorentz-invariant quantity. In addition, in [2] a new variable was introduced, defined as

$$\hat{s}_{\min}^{1/2}(M_{\mathrm{inv}}) \equiv \sqrt{M^2 + \not{E}_T^2} + \sqrt{M_{\mathrm{inv}}^2 + \not{E}_T^2} \,, \tag{1.2}$$

where the parameter $M_{\mathrm{inv}}$ is a variable estimating the sum of masses of all invisible particles in the event:

$$M_{\mathrm{inv}} \equiv \sum_{i=1}^{n_{\mathrm{inv}}} m_i \,. \tag{1.3}$$

It was argued that the peak in the distribution of $\hat{s}_{\min}^{1/2}$ is a good indicator of the mass scale of new physics processes involving heavy particle production.

In ref. [1] we examined the effects of QCD initial state radiation (ISR) on these observables, first in an approximate fixed-order treatment, taking into account collinear-enhanced terms, and then in an all-orders resummation of such terms. We quantified the way the distributions of quantities that involve longitudinal momenta depend on the scale of the underlying hard subprocess and on the properties of the detector, in particular the maximum visible pseudorapidity $\eta_{\mathrm{max}}$.

In the treatment in ref. [1] we supposed that all the final-state particles from the hard subprocess are detected. We considered in detail the case of top quark pair production when both the $t$ and $\bar{t}$ decay hadronically. In the present paper we study the effect of invisible particle emission, which allows us to extend the validity of our treatment to many cases of Standard Model and beyond Standard Model processes of interest at the LHC. We examine semi-leptonic/hadronic and fully semi-leptonic decays of the top quark (see Fig. 1). We also consider gluino pair-production, where the final decay products contain heavy invisible particles, the lightest supersymmetric particles (LSPs), which remain undetected. The emission of the LSPs in the decay of the gluino can cause a sizeable effect on global inclusive observables. We examine the interplay of this effect with ISR effects.
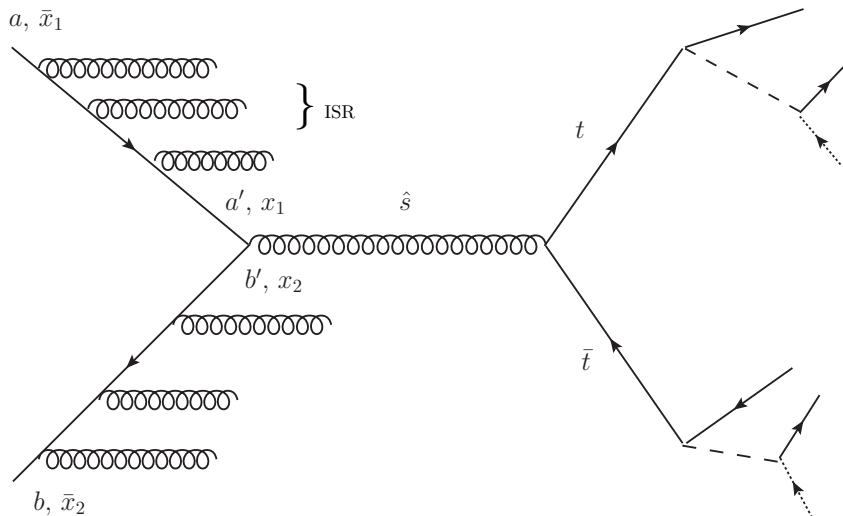
**Figure 1:** Feynman diagram for $qq' + \mathrm{ISR} \to g \to t\bar{t} \to jjll\not{E}_T$. The solid lines represent visible jets or leptons, the dotted lines invisible neutrinos.

The Monte Carlo results presented in refs. [1,2] show that the second term on the right-hand side of eq. (1.2) is not strongly affected by ISR. The first term is intended to add extra longitudinal information about the hard subprocess, allowing a more reliable determination of its mass scale. The extra information enters through the visible mass $M$. Therefore, as in ref. [1], we concentrate on this quantity.

The paper is organised in the following way: In section 2 we review the ISR resummation. Then in section 3 we develop our treatment of ISR effects to include one or two invisible decays originating from the hard process. In section 4 we present comparisons of resummed distributions to distributions produced using the general-purpose Monte Carlo event generator `Herwig++` [3] for $t\bar{t}$ and $\tilde{g}\tilde{g}$ production. Moreover, we examine the effect of hadronization of ISR and the effect of the underlying event on the parton-level distributions. Our conclusions are summarized in section 5. Appendix A contains details of the numerical Mellin inversion method used to obtain the evolution kernels and appendix B gives the parton-level cross sections for the processes under investigation.

## 2. ISR effects without invisible particle emission

We first review briefly the main results of ref. [1]. Consider the emission of ISR partons from incoming partons $a$ and $b$, as in Fig. 1. If all the products of the hard subprocess and all the ISR emitted at angles greater than $\theta_c$ are detected, the resummed differential cross section may be written as:

$$M^2 \frac{d\sigma_{ab}}{dM^2 dY} = \int dx_1 \, dx_2 \, K_{a'a}(x_1/\bar{x}_1) f_a(\bar{x}_1, Q_c) \, K_{b'b}(x_2/\bar{x}_2) f_b(\bar{x}_2, Q_c) \, \hat{\sigma}_{a'b'}(x_1 x_2 S) \ ,$$

(2.1)

or equivalently

$$S\frac{d\sigma_{ab}}{dM^2dY} = \int dz_1\,dz_2\,K_{a'a}(z_1)f_a(\bar{x}_1, Q_c)\,K_{b'b}(z_2)f_b(\bar{x}_2, Q_c)\,\hat{\sigma}_{a'b'}(z_1z_2M^2)\ ,\quad (2.2)$$

where $M$ and $Y$ are the invariant mass and rapidity of the detected system (the 'visible' mass and rapidity) and

$$\bar{x}_1 = \frac{M}{\sqrt{S}}e^Y\ ,\quad \bar{x}_2 = \frac{M}{\sqrt{S}}e^{-Y}\ ,\quad (2.3)$$

$\sqrt{S}$ being the overall c.m. energy-squared. The hard subprocess cross section $\hat{\sigma}_{a'b'}$ is evaluated at c.m. energy squared $Q^2 = x_1x_2S = z_1z_2M^2$, where $z_i = x_i/\bar{x}_i$. The parton distribution functions (PDFs) $f_{a,b}$ are evaluated at the lower scale $Q_c \sim \theta_c Q$.[1] The kernel functions $K_{a'a}$ and $K_{b'b}$ describe the evolution of the PDFs from scale $Q_c$ to $Q$. They satisfy an evolution equation like that of the parton distributions themselves:

$$Q\frac{\partial}{\partial Q}K_{b'b}(z) = \frac{\alpha_{\rm S}(Q)}{\pi}\int\frac{dz'}{z'}P_{b'a}(z')K_{ab}(z/z')\ ,\quad (2.4)$$

with the initial condition that $K_{ab}(z) = \delta_{ab}\delta(1-z)$ at $Q = Q_c$. We describe in appendix A the method that we used to compute the kernel functions.

The main conclusions from the study in ref. [1] are that, in the absence of invisible particles, the above analytical results are in good agreement with those of Monte Carlo simulations, and that the distribution of the new variable (1.2) is indeed determined primarily by that of the visible mass $M$.

## 3. ISR effects including invisible particle emission

Suppose now that an invisible 4-momentum $p_{inv}^{\mu}$ is emitted from the hard subprocess. If we define the total lab-frame 4-momentum of the incoming partons $a$ and $b$ as $P^{\mu} = (E, \vec{P})$,

$$P^{\mu} = \frac{1}{2}\sqrt{S}[(\bar{x}_1 + \bar{x}_2), 0, 0, (\bar{x}_1 - \bar{x}_2)]\ ,\quad (3.1)$$

then the visible 4-momentum will be $P^{\mu} - p_{inv}^{\mu}$. By definition, the visible mass is then given by:

$$M^2 = (P - p_{inv})^2 = P^{\mu}P_{\mu} + p_{inv}^{\mu}p_{inv,\mu} - 2p_{inv}^{\mu}P_{\mu}\ .\quad (3.2)$$

Equation (3.2) demonstrates the interplay between two effects: on one hand ISR increases the 'true' scale of the hard process $Q$, to the 'apparent' scale $M$ by contaminating the detector with extra particles, and on the other hand the invisible

---

[1]We find that results are somewhat sensitive to the constant of proportionality here. We actually use $Q_c = Q\exp(-\eta_{\rm max})$ where $\eta_{\rm max} = -\ln\tan(\theta_c/2)$ is the maximum visible pseudorapidity.

particle emission decreases $M$ by the loss of particles. In the case of gluino pair-production both effects are equally important, as we will show.

Substituting from eq. (3.1) in eq. (3.2) and defining $p_{inv}^{\pm} = p_{inv}^0 \pm p_{inv}^3$ we obtain

$$M^2 = \bar{x}_1 \bar{x}_2 S + m_{inv}^2 - \sqrt{S}[\bar{x}_1 p_{inv}^- + \bar{x}_2 p_{inv}^+] , \qquad (3.3)$$

where $m_{inv}$ represents the total invariant mass of the invisibles, $m_{inv}^2 = p_{inv}^\mu p_{inv,\mu}$.

The momenta $p_{inv}^\mu$ are defined in the lab frame, relative to which the c.m. frame of the hard subprocess is boosted by an amount defined by the momentum fractions $x_1$ and $x_2$ of the partons entering the subprocess. This implies that the $p_{inv}^{\pm}$ transform as:

$$p_{inv}^+ = \sqrt{\frac{x_1}{x_2}} q_{inv}^+ , \quad p_{inv}^- = \sqrt{\frac{x_2}{x_1}} q_{inv}^- , \qquad (3.4)$$

where $q_{inv}^{\pm} = q_{inv}^0 \pm q_{inv}^3$, defined in terms of the invisible momentum, $q_{inv}^\mu$, in the c.m. frame of the hard subprocess. Substituting the expressions of eq. (3.4) in eq. (3.3) we find an expression for the visible invariant mass:

$$M^2 = m_{inv}^2 + \bar{x}_1 \bar{x}_2 S \left[ 1 - z_1 f_{inv}^+ - z_2 f_{inv}^- \right] , \qquad (3.5)$$

where we have defined $f_{inv}^{\pm} = q_{inv}^{\pm}/Q$ and used $Q^2 = \bar{x}_1 \bar{x}_2 z_1 z_2 S$. We may now solve eq. (3.5) for $Q^2$ to obtain $Q^2$ in terms of $M^2$:

$$Q^2 = \frac{z_1 z_2 (M^2 - m_{inv}^2)}{1 - z_1 f_{inv}^+ - z_2 f_{inv}^-} . \qquad (3.6)$$

The above expression for the hard subprocess scale now becomes the argument of the parton-level cross section, $\hat{\sigma}_{a'b'}$ in eq. (2.2):

$$S\frac{d\sigma_{ab}}{dM^2 dY} = \int dz_1\, dz_2\, K_{a'a}(z_1) f_a(\bar{x}_1, Q_c)\, K_{b'b}(z_2) f_b(\bar{x}_2, Q_c)\, \hat{\sigma}_{a'b'} \left( \frac{z_1 z_2 (M^2 - m_{inv}^2)}{1 - z_1 f_{inv}^+ - z_2 f_{inv}^-} \right) . \qquad (3.7)$$

The functions $f_{inv}^{\pm}$, which are related to the invisible particle four-momenta, remain to be determined. The visible system rapidity, $Y$, is also modified by the presence of invisible particles as:

$$Y = \frac{1}{2} \log \left( \frac{\bar{x}_1 (1 - z_1 f_{inv}^+)}{\bar{x}_2 (1 - z_2 f_{inv}^-)} \right) , \qquad (3.8)$$

and therefore eqs. (2.3) for $\bar{x}_{1,2}$ become

$$\bar{x}_1 = \sqrt{\frac{(M^2 - m_{inv}^2)(1 - z_2 f_{inv}^-)}{S(1 - z_1 f_{inv}^+ - z_2 f_{inv}^-)(1 - z_1 f_{inv}^+)}} e^Y ,$$

$$\bar{x}_2 = \sqrt{\frac{(M^2 - m_{inv}^2)(1 - z_1 f_{inv}^+)}{S(1 - z_1 f_{inv}^+ - z_2 f_{inv}^-)(1 - z_2 f_{inv}^-)}} e^{-Y} . \qquad (3.9)$$

The kinematic constraints restrict $Q^2$ to be greater than the threshold energy squared for the process and the true invariant mass, $M_{true}^2 \equiv \bar{x}_1 \bar{x}_2 S = Q^2/(z_1 z_2)$, to be greater than the visible invariant mass, $M^2$. These result in the following constraints for $Q^2$:

$$Q^2 > Q_{threshold}^2 \ , \quad Q^2 > z_1 z_2 M^2 \ . \tag{3.10}$$

## 3.1 Single-invisible decays

The benchmark scenario for a single invisible decay originating from the hard process is $t\bar{t}$ production in which one of the two tops decays into $bqq'$ (hadronic) and the other into $b\ell\nu$ (semi-leptonic), the neutrino comprising the missing four-momentum. Excluding the proton remnants, we assume that all other particles within the pseudo-rapidity coverage are detected. We will refer to the neutrino as the invisible particle and the $W$ as the intermediate particle in the $t\bar{t}$ case, but the treatment is readily applicable to the gluino case where the invisible particle is the $\chi_1^0$ and the intermediate particle is a squark (treated in section 3.2).

To calculate the functions $f_{inv}^{\pm}$ and obtain $Q^2$, we need to calculate the neutrino four-momentum in the hard process frame. This is done by choosing the neutrino four-momentum in the frame of its parent $W$ and then applying two subsequent Lorentz boosts: one going from the $W$ frame to the top frame, and one from the top frame to the hard process frame. The decay chain is shown in Fig. 3.1. Each of these boosts involves two angular variables which originate from the 'decay' of the parent particle. Hence the four momentum $q_{inv}^{\mu}$ of the neutrino may be written as

$$q_{inv}^{\mu} = \Lambda_{\kappa}^{\mu}\left(Q, \hat{\theta}, \hat{\phi}\right) \Lambda_{\lambda}^{\kappa}\left(\tilde{\theta}, \tilde{\phi}\right) \bar{p}_{\nu}^{\lambda}(\bar{\theta}, \bar{\phi}) \ , \tag{3.11}$$

where the $\Lambda$'s are Lorentz boost matrices and where quantities with a hat refer to the hard process frame, quantities with a tilde refer to the top frame and quantities with a bar refer to the $W$ frame. The angles $\theta$ and $\phi$ represent the usual polar angles, defined with respect to the direction of the 'sister' particle (see Fig. 3.1). For example, in the case $W^+ \to \ell^+ \nu_\ell$, where the $W^+$ was produced from the top decay along with a bottom quark, the angles $(\bar{\theta}, \bar{\phi})$ are defined with respect to the direction of motion of the $b$ in the $W^+$ frame. The two boost vectors have magnitudes given by $|\vec{\beta}_i| = |\vec{p}_i|/E_i$ ($i = t, W$), the ratio of the parent 3-momentum magnitude and its energy. The boosts, as well as the magnitude of the invisible particle four-momentum, can obtained by considering kinematics in each frame as:

$$\bar{p}_{\nu}^{\lambda}(\bar{\theta}, \bar{\phi}) = \frac{m_W}{2}(1, \vec{\bar{r}}) \ , \tag{3.12}$$

$$\vec{\beta}_W = \frac{m_t^2 - m_W^2}{m_t^2 + m_W^2} \vec{\tilde{r}} \ ,$$

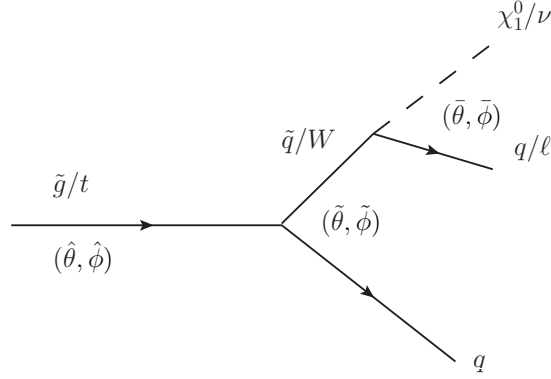$$\vec{\beta}_t = \sqrt{1 - \frac{4m_t^2}{Q^2}} \vec{\hat{r}} \ ,$$

**Figure 2:** The sequential two-body decay chain under consideration in the invisible particle treatment. The relevant production angles in the parent centre-of-mass frame are also shown in parentheses.

where $\vec{r} = (\sin\theta\cos\phi, \sin\theta\sin\phi, \cos\phi)$ is the unit vector in spherical polar coordinates in the appropriate frame and $m_W$, $m_t$ are the $W$ and top quark masses respectively. The four-vector $f_{inv}^{\mu}$, and hence the functions $f_{inv}^{\pm}$, are calculated by $f_{inv}^{\pm} = q_{inv}^{\pm}/Q$. Evidently, the functions $f_{inv}^{\pm}$ are functions of $Q^2$, giving an implicit equation for $Q^2$. To make this more explicit, we re-write eq. (3.6):

$$Q^2 = \frac{z_1 z_2 \left[M^2 - m_{inv}^2(Q^2, \Omega)\right]}{1 - z_1 f_{inv}^+(Q^2, \Omega) - z_2 f_{inv}^-(Q^2, \Omega)} \ , \tag{3.13}$$

and analogously for eq. (3.9), where $\Omega$ represents the set of all angular variables. In the present case $m_{inv}(Q^2, \Omega) = m_\nu \simeq 0$ but for multiple invisible particles it will also be a function as indicated.

Equation (3.13) needs to be solved numerically for each set $(z_1, z_2, \Omega)$ in the region $(4m_{t/\tilde{g}}^2, z_1 z_2 S)$, where $S$ is the square of the proton centre-of-mass energy, along with the restriction that the visible invariant mass should be lower than the 'true' invariant mass, $M \leq M_{true}$. The numerical solution was found using the Van Wijngaarden-Dekker-Brent method [4, 5], a bracketing method for finding roots of one-dimensional equations. Since $Q$ is not uniquely determined for each $M$, different values of the 'true' centre-of-mass energy $Q$ contribute to the cross section. Note that not all possible configurations $(z_1, z_2, \Omega)$ are kinematically allowed to contribute to the cross section at $M$ and hence some configurations do not yield roots of eq. (3.13). Once $Q^2$ is obtained, the parton-level cross section for the hard process partons, $\hat{\sigma}_{a'b'}(Q^2)$, is calculated. This result is then multiplied with the parton density functions for the incoming partons, $f_{a,b}(\bar{x}_{1,2}, Q_c)$, and the kernels for evolution from incoming partons $a$ and $b$ to hard process partons $a'$ and $b'$ ($K_{a'a}(z_1)$ and $K_{b'b}(z_2)$). We then integrate over all possible values of $z_1$ and $z_2$, according to eq. (3.7). Finally, to obtain the full resummed result we have to integrate over the distribution of the angular variables $\Omega$. Notice that the visible invariant mass distri-

bution becomes non-zero below the threshold for production, $M < 2m_{t/\tilde{g}}$, owing to the loss of invisible particles.

## 3.2 Double-invisible decays

We now turn to the case where both particles produced in the hard process decay invisibly. For illustration we refer to sequential decays of the gluino: $\tilde{g} \to \tilde{q}q \to \chi_1^0 qq$. Although this decay mode is generally not the dominant one, it is useful for illustration of the procedure. We extend the treatment given in the semi-leptonic/hadronic top case by writing out functions related to the two invisible particle four-momenta in the decay chain (which we call $\chi$ and $\chi'$),

$$q_\chi^\mu = \Lambda_\kappa^\mu \left(Q, \hat{\theta}, \hat{\phi}\right) \Lambda_\lambda^\kappa \left(\tilde{\theta}, \tilde{\phi}\right) \bar{p}_\chi^\lambda(\bar{\theta}, \bar{\phi}) \,, \tag{3.14}$$

$$q_{\chi'}^\mu = \Lambda_\kappa^\mu \left(Q, \hat{\theta}', \hat{\phi}'\right) \Lambda_\lambda^\kappa \left(\tilde{\theta}', \tilde{\phi}'\right) \bar{p}_{\chi'}^\lambda(\bar{\theta}', \bar{\phi}') \,, \tag{3.15}$$

where the primed quantities now distinguish between the two invisibles. Since both of these four-vectors are defined in the hard subprocess frame, we have simply

$$f_{inv}^\pm = \frac{1}{Q} \left(q_\chi^\pm + q_{\chi'}^\pm\right) \,. \tag{3.16}$$

The rest of the treatment is identical to the one-invisible case: an implicit equation has to be solved to obtain $Q^2$ for each $(z_1, z_2, \Omega)$ set and then an integral over $\Omega$ is taken to obtain the resummed result.

## 3.3 Angular distributions

The distributions of the angular variables $\Omega = (\hat{\theta}, \hat{\phi}, \tilde{\theta}, \tilde{\phi}, \bar{\theta}, \bar{\phi})$, appearing in the treatment of invisibles given in the previous sections, are process-dependent. They represent the angles at which the daughter particle is emitted in the frame of the parent particle. We investigated the angular distributions using a Monte Carlo event generator (`Herwig++` 2.4.0 [3]) and subsequently used the results in calculating the $f_{inv}^\pm$ functions. The results for SPS1a gluino pair-production are shown in Fig. 3, where the uniform distributions are shown for comparison (red horizontal line). Figure 4 shows the distributions as obtained for top pair-production. The neutrino angle in the $W$ frame is also compared to the analytic calculation. As expected, all the $\phi$ angles, in both cases, were found to be uniform (not shown). The form of all the distributions can be justified using general spin considerations:

$\hat{\theta}_i$: The angular distribution of the angle $\hat{\theta}_i$ at which the fermions are produced in the hard process frame is expected to have the form $\sim 1 + \beta \cos^2 \hat{\theta}_i$, where $\beta$ is a process-dependent constant.

$\tilde{\theta}_i$: The angle $\tilde{\theta}_i$, is defined between the direction of the daughter boson ($W$ or $\tilde{q}$) with respect to the direction of polarization of the parent ($t$ or $\tilde{g}$) polarization. The angular distribution for a spin-up fermion parent is then given by [6]:

$$\frac{1}{N_\uparrow}\frac{\mathrm{d}N_\uparrow}{\mathrm{d}\cos\tilde{\theta}_i} = \frac{1}{2}(1 + P\alpha_i\cos\tilde{\theta}_i) \ , \tag{3.17}$$

where $\alpha_i$ is a constant and $P$ is the modulus of the polarization of the parent. Since the production processes for both $t\bar{t}$ and $\tilde{g}\tilde{g}$ are parity conserving, there is also an equal spin-down ($N_\downarrow$) contribution to the total distribution with the sign of $\alpha_i$ reversed. This results in a uniform distribution for $\cos\tilde{\theta}_i$.
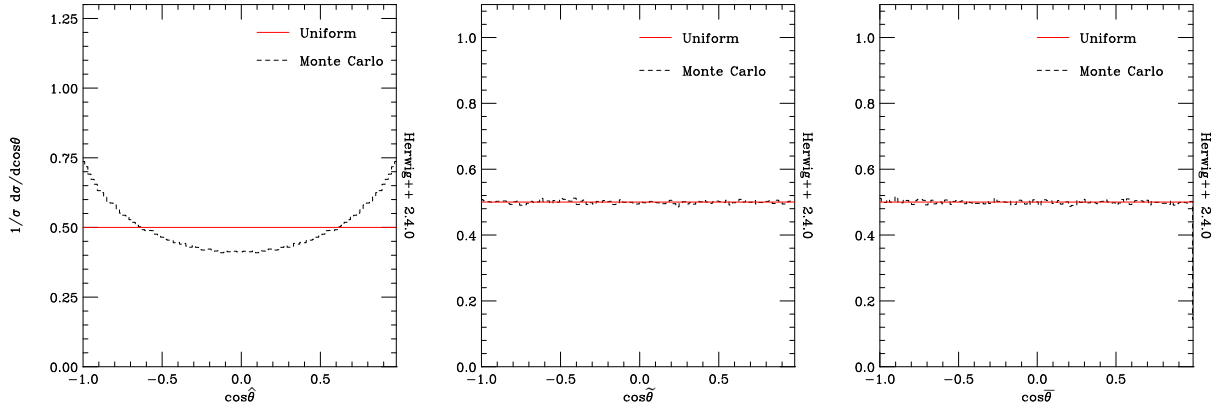


**Figure 3:** Monte Carlo results for the gluino pair-production decay chain angles. From left to right: the production angle of the gluino in the hard process frame, the angle of the outgoing squark in the gluino frame and the angle of the outgoing neutralino in the squark frame. The uniform distributions are shown for comparison.

$\bar{\theta}_i$: In gluino pair-production, the decay products of the squark, $\tilde{q}$, which is a scalar, are uniformly distributed in $\cos\bar{\theta}$. In top pair-production, on the other hand, the decay $W \to \ell\nu_\ell$ is parity-violating and the distribution of $\cos\bar{\theta}$ is forward-backward asymmetric in the $W$ frame [7]. The angle $\bar{\theta}$ (sometimes called $\Psi$, see e.g. [8]) is used experimentally to infer helicity information on the $W$. The distribution may be written as

$$\frac{1}{N}\frac{\mathrm{d}N}{\mathrm{d}\cos\bar{\theta}} = \frac{3}{2}\left[F_0\left(\frac{\sin\bar{\theta}}{\sqrt{2}}\right)^2 + F_L\left(\frac{1-\cos\bar{\theta}}{2}\right)^2 + F_R\left(\frac{1+\cos\bar{\theta}}{2}\right)^2\right] \ , \tag{3.18}$$

where $F_L$, $F_R$ and $F_0$ are the probabilities for left-handed, right-handed and longitudinal helicities of the $W$ in top quark decay respectively. The SM predictions, $(F_L, F_R, F_0) = (0.304, 0.001, 0.695)$, yield the curve shown on the right in Fig. 4.
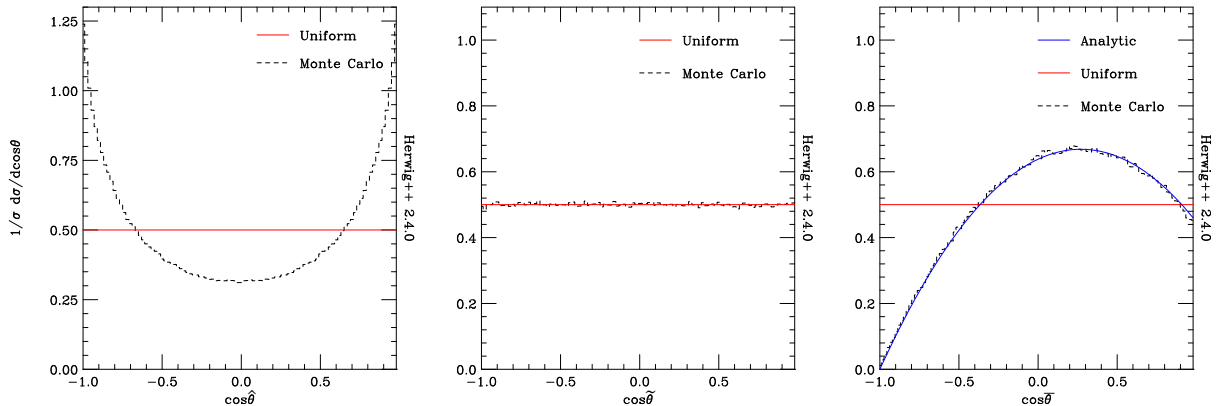
**Figure 4:** Monte Carlo results for the top pair-production decay chain angles. From left to right: the production angle of the top in the hard process frame, the angle of the outgoing $W$ boson in the top frame and the angle of the outgoing neutrino in the $W$ frame. The uniform distributions are shown for comparison. The neutrino angle in the $W$ frame is also compared to the analytic calculation.

The spins of the two produced fermions (tops or gluinos) are correlated and this may cause a degree of correlation between the distributions of particles in the decay chains. We investigated whether these correlations play an important role in the calculation of the invisible particle effects on the visible mass. By comparing the invariant mass distributions with and without the spin correlations in the Monte Carlo we concluded that the effect is small in both top and gluino pair-production and can be safely neglected.

## 4. Results

We present the resummed distributions obtained for $t\bar{t}$ and $\tilde{g}\tilde{g}$ production according to eq. (3.7). All results are for the LHC at design energy, i.e. $pp$ collisions at $\sqrt{s} = 14$ TeV. We have integrated over the visible system rapidity, $Y$, in the range $|Y| < 5$. We first compare our results to those obtained using the `Herwig++` event generator at parton level (i.e. no hadronization or underlying event) and excluding the proton remnants.[2] In sections 4.3 and 4.4 we examine the effects of hadronization and the underlying event. Parton-level top and gluino pair-production cross section formulae are given in appendix B. The PDF set used both in the calculation and `Herwig++` is the MRST LO** (MRSTMCal) set [9, 10].

### 4.1 Top quark pair production

We present resummed results in comparison to Monte Carlo for Standard Model $t\bar{t}$ production, where we include particles with maximum pseudorapidity $\eta_{\max} = 5$. In

---

[2]We verified using the event generator that the contribution of the proton remnants to the total invariant mass in the considered rapidity range is negligible.
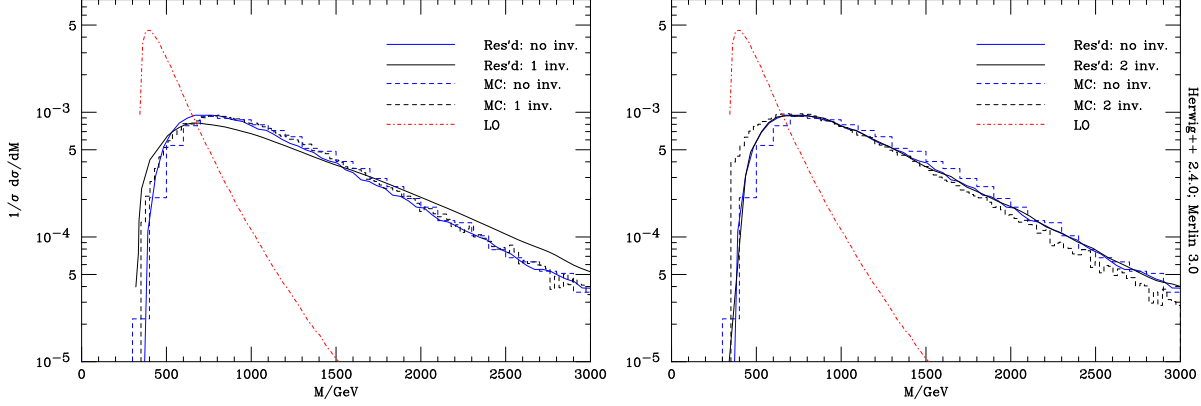
**Figure 5:** The $t\bar{t}$ visible mass distributions for a pseudorapidity cut $\eta_{\mathrm{max}} = 5$. Left: comparing hadronic (no invisibles) and semi-leptonic (one invisible) decays. Right: comparing hadronic (no invisibles) and fully leptonic (two invisibles) decays. The leading order $t\bar{t}$ invariant mass distribution is shown (red dot dashes) for comparison.

Fig. 5 we show separate results for combinations of hadronic and semi-leptonic decays of the top, leading to zero, one or two invisible neutrinos from the hard process. The effect of the invisibles in both the fully semi-leptonic case and the hadronic/semi-leptonic case are small compared to the effects of hadronization, to be discussed in section 4.3. The differences between the Monte Carlo and resummed curves in Fig. 5 may be attributed to sensitivity to the behaviour of the PDFs and parton showering at low scales, and the precise definition of $Q_c$ in terms of $\eta_{\mathrm{max}}$, since $Q_c$ can be as low as $2m_t \times e^{-5} \sim 2$ GeV in the case of $t\bar{t}$ production.

## 4.2 Gluino pair production

We focus on the SPS1a point [11], which has gluino and lightest neutralino masses $m_{\tilde{g}} = 604.5$ GeV and $m_{\chi_1^0} = 97.0$ GeV respectively (and see table 1 for the squark masses). For simplicity we set the squark mass in the invisible particle treatment to 550 GeV. We also present results for a modified SPS1a point, with $m_{\tilde{g}} = 800$ GeV. In this process only the two-invisibles case is realistic, but for comparison we also show results for no invisibles, i.e. imagining that the two lightest neutralinos are also detected. When $\eta_{\mathrm{max}} = 5, 3$, there is fairly good agreement between the Monte Carlo and resummation predictions in both the two-invisibles and no-invisibles cases, and for both gluino masses, as shown in Figs. 6 and 7, where one should compare the dashed histograms (Monte Carlo) to the solid curves of the same colour (resummation).

The shift in the peak of the visible mass distribution in going from no to two invisibles is much larger than that in top pair production, amounting to 600-700 GeV, roughly independent of $\eta_{\mathrm{max}}$ and the gluino mass. This results mainly from the higher masses of the intermediate particles in the decays ($m_{\tilde{q}} \simeq 550$ GeV vs. $m_W = 80$ GeV), which implies a higher energy release, rather than the masses of the

| Particle | Mass (GeV) | Particle | Mass (GeV) |
|:---:|:---:|:---:|:---:|
| $\tilde{g}$ | 604.5 | $\tilde{s}_L$ | 570.7 |
| $\chi_1^0$ | 97.0 | $\tilde{s}_R$ | 547.9 |
| $\tilde{u}_L$ | 562.3 | $\tilde{b}_1$ | 515.3 |
| $\tilde{u}_R$ | 548.2 | $\tilde{b}_2$ | 547.7 |
| $\tilde{d}_L$ | 570.7 | $\tilde{t}_1$ | 400.7 |
| $\tilde{d}_R$ | 547.9 | $\tilde{t}_2$ | 586.3 |

**Table 1:** The relevant particle masses in the supersymmetric model used in the invisible study, SPS1a. The modified SPS1a point differs in that it has $m_{\tilde{g}} = 800$ GeV.

invisible particles themselves ($m_{\chi_1^0} = 97$ GeV vs. $m_\nu = 0$).

One of the assumptions of the resummation is that all the visible hard process decay products are detected, which is not true when the maximum pseudorapidity $\eta_{\max}$ is restricted to lower values. When $\eta_{\max} \sim 2$ in the Monte Carlo analysis, a significant number of hard process particles begin to be excluded and hence the curves shift to lower values than the resummed predictions. Figure 8 shows the rapidity distribution of the decay products of the gluino at parton level for $m_{\tilde{g}} = 604.5$ GeV. For the case shown, cuts of $\eta_{\max} = 5, 3, 2$ and 1.4 correspond to exclusion of, respectively, $\sim$0.002%, 1.1%, 7.5% and 20.0% of the gluino decay products from the detector. The effect of this appears in Figs. 9 and 10, where the Monte Carlo distributions are narrower and peak at lower masses than the resummed predictions. The variation between the resummed $\eta_{\max} = 2$ and 1.4 curves is smaller than that between $\eta_{\max} = 5$ and 3, since they correspond to smaller differences in $Q_c$.

The heavy and light gluino scenarios exhibit similar behaviour when varying the pseudorapidity coverage and the number of invisibles, showing the lack of dependence of the resummation on the mass of the pair-produced particle. The sensitivity to low-scale PDF behaviour and showering is reduced compared to the $t\bar{t}$ case since we are considering higher centre-of-mass energies, with the lowest possible $Q_c$ now being of the the order $2m_{\tilde{g}} \times e^{-5} \sim 8$ GeV. The position of the curves is also sensitive to the precise definition of $Q_c$ in terms of $\eta_{\max}$.

Table 2 shows a summary of the peak positions for all cases and different pseudorapidity cuts. For the higher values of $\eta_{\max}$, the agreement between the Monte Carlo and resummation is satisfactory. There is a large difference in the peak positions for no invisibles and $\eta_{\max} = 5$, but this is mainly due to the broad shape of the peak in this case, while the overall distributions agree better. For $\eta_{\max} \leq 2$ there is a growing discrepancy, especially for the realistic case of two invisibles, due to the loss of particles coming from the hard process.

| $m_{\tilde{g}}$ (GeV). | $\eta_{\max}$ | MC (GeV) (0 inv./2 inv.) | Resum. (GeV) (0 inv./2 inv.) |
|---|---|---|---|
| 604.5 | 5 | 2280/1560 | 1785/1620 |
| 604.5 | 3 | 1680/1080 | 1593/1204 |
| 604.5 | 2 | 1440/840 | 1497/1204 |
| 604.5 | 1.4 | 1380/660 | 1497/1204 |
| 800.0 | 5 | 2820/2100 | 2569/1870 |
| 800.0 | 3 | 2220/1620 | 2128/1684 |
| 800.0 | 2 | 1920/1380 | 1865/1683 |
| 800.0 | 1.4 | 1740/1140 | 1865/1683 |

**Table 2:** Summary of the positions of the peaks of the gluino pair-production visible mass distributions as given by the Monte Carlo and the resummation, for different values of the maximum pseudorapidity and for no and two invisibles.

## 4.3 Hadronization effects

We have assumed that ISR partons emitted at pseudorapidities above $\eta_{\max}$ do not contribute to the visible invariant mass. This would be true if the hadronization process were perfectly local in angle. However, as a result of hadronization high-rapidity ISR partons can produce lower-rapidity hadrons and thus 'contaminate' the detector and shift the visible mass to higher values.

The hadronization model employed in the `Herwig++` Monte Carlo is a refinement of the cluster model described in ref. [12]. The model involves clustering of partons into colour-singlet objects that decay into hadrons, resulting in a smearing of the pseudorapidity distribution which causes the increase in the visible mass described above. The effect is shown in Fig. 11 for gluino and top pair-production (excluding
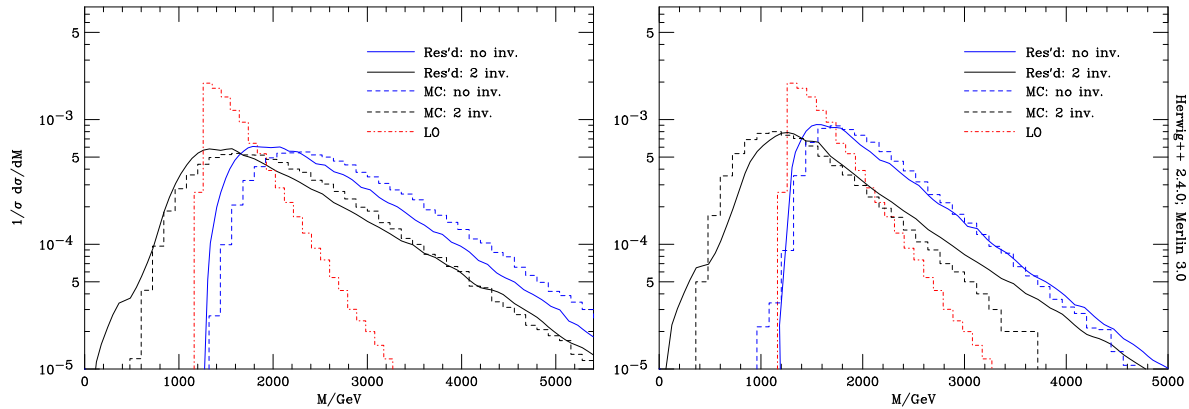


**Figure 6:** The SPS1a gluino pair-production visible mass distributions for pseudorapidity cuts $\eta_{\max} = 5$ (left) and $\eta_{\max} = 3$ (right). The leading order distribution is shown (red dot dashes) for comparison.
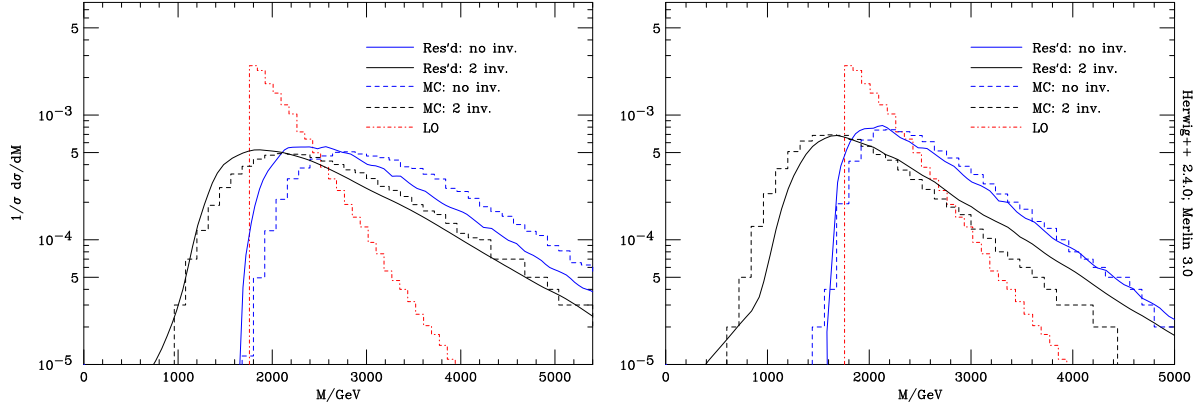
**Figure 7:** The modified SPS1a gluino pair-production (with $m_{\tilde{g}} = 800$ GeV) results for pseudorapity cuts $\eta_{\max} = 5$ (left) and $\eta_{\max} = 3$ (right) . The leading order distribution is shown (red) for comparison.

the invisible particles from the hard process). The effect was found to be larger for $t\bar{t}$ production where the mass distribution is shifted significantly, whereas in gluino pair production the shift is negligible.

## 4.4 Underlying event

The underlying event, which is thought to arise from multiple soft interactions of spectator partons, is a further source of non-perturbative contributions to the visible mass. If $P_H^\mu$ represents the "hard" visible 4-momentum studied in earlier sections and $P_U^\mu$ represents that due to the underlying event, the total visible mass is given
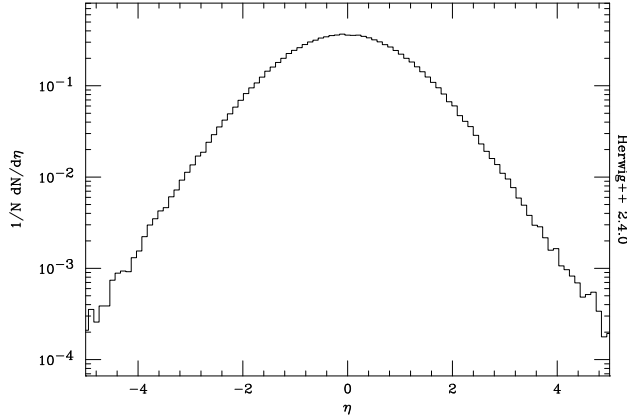


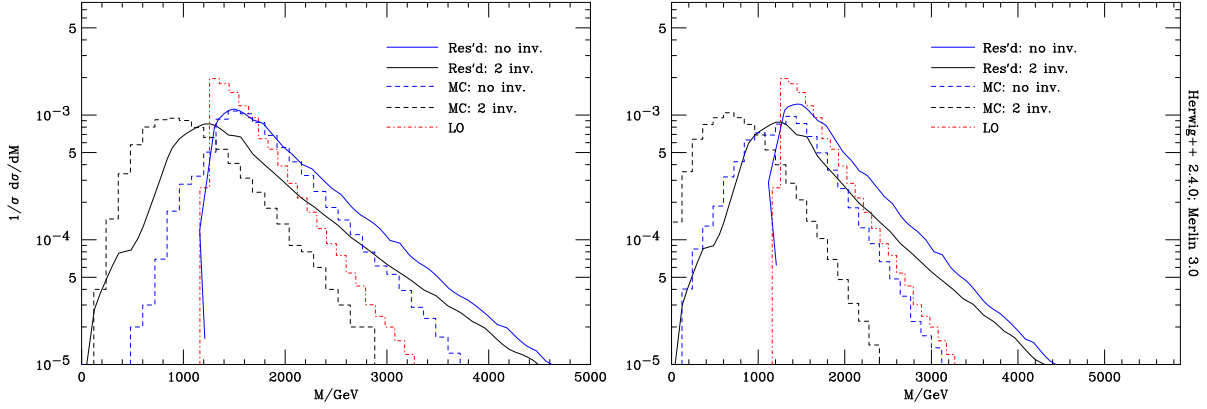**Figure 8:** The SPS1a gluino pair-production pseudorapidity distribution for $m_{\tilde{g}} = 604.5$ GeV.

**Figure 9:** The SPS1a gluino pair-production results for pseudorapidity cuts $\eta_{\max} = 2$ (left) and $\eta_{\max} = 1.4$ (right). The leading order distribution is shown (red dot dashes) for comparison.

by

$$
\begin{aligned}
M^2 = (P_H + P_U)^2 &= M_H^2 + M_U^2 + 2(E_H E_U - P_{zH} P_{zU}) \\
&= M_H^2 + M_U^2 + 2 M_U \sqrt{M_H^2 + \not{E}_T^2} \cosh(Y_H - Y_U) \,. \qquad (4.1)
\end{aligned}
$$

where we neglect transverse momentum associated with the underlying event. Thus, even if the visible invariant mass due to the underlying event is small, its effect on the overall visible mass may be enhanced through the last term on the right-hand side.

The underlying event is simulated in `Herwig++` by a multiple parton interaction model along the lines of ref. [13]. In this model, for the rapidity ranges considered here, the underlying event is approximately process-independent and exhibits little
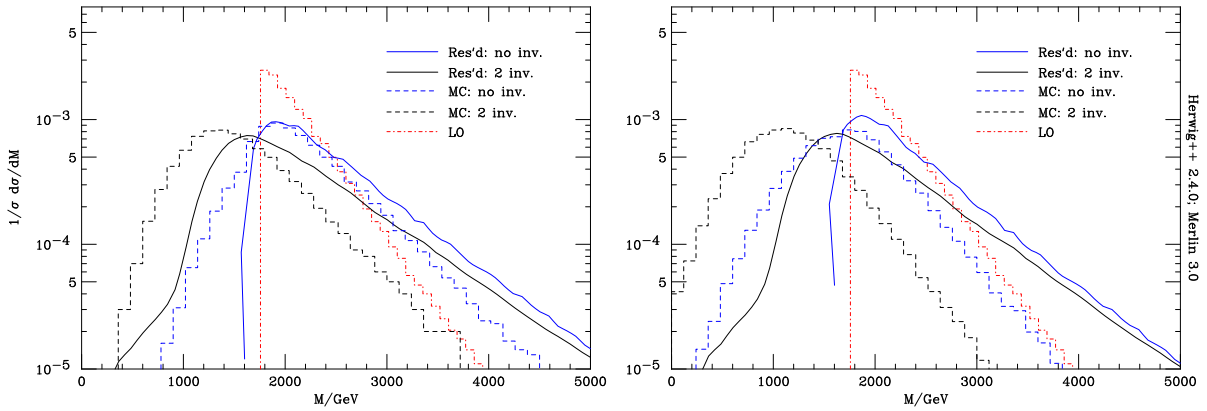


**Figure 10:** The modified SPS1a gluino pair-production (with $m_{\tilde{g}} = 800$ GeV) results for pseudorapity cuts $\eta_{\max} = 2$ (left) and $\eta_{\max} = 1.4$ (right). The leading order distribution is shown (red) for comparison.
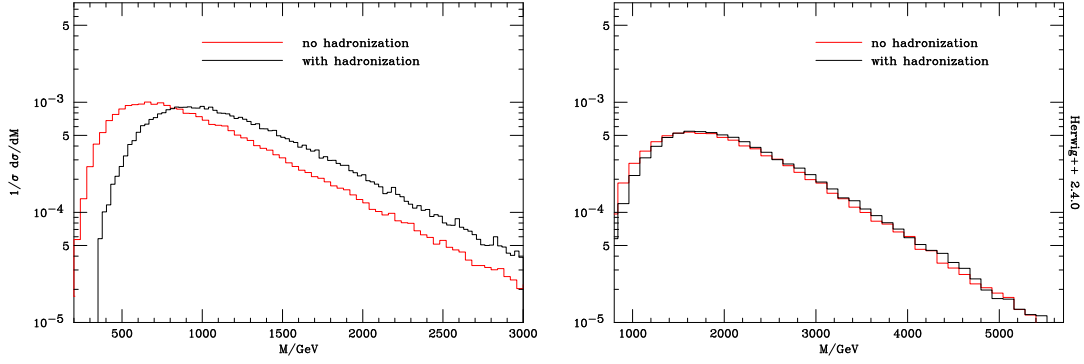
**Figure 11:** The $t\bar{t}$ fully semi-leptonic (left) and SPS1a gluino pair-production (right, with $m_{\tilde{g}} = 604.5$ GeV) visible mass distributions for a pseudorapity cut $\eta_{\max} = 5$ with and without hadronization (black and red respectively).

correlation with the rest of the event. Therefore, to a good approximation, the distributions of the variables related to the underlying event, $Y_U$ and $M_U$, can be determined once and for all at each collider energy. The process-dependence comes primarily through the dependence on $Y_H$ and $M_H$, which can be calculated using the resummation formula given in eq. (3.7). The overall visible mass distribution can then be obtained by convolution using eq. (4.1).

The effects of including the underlying event in the visible mass distribution are shown in Figs. 12 and 13 for $t\bar{t}$ and gluino pair production, respectively. The multiple parton interactions push the peak value to substantially higher masses. The shift amounts to about 250 GeV at $\eta_{max} = 3$ and 1.2 TeV at $\eta_{max} = 5$, and is roughly process-independent. However, since the underlying event is approximately uncorrelated with the hard process, the visible mass distributions can be reconstructed well
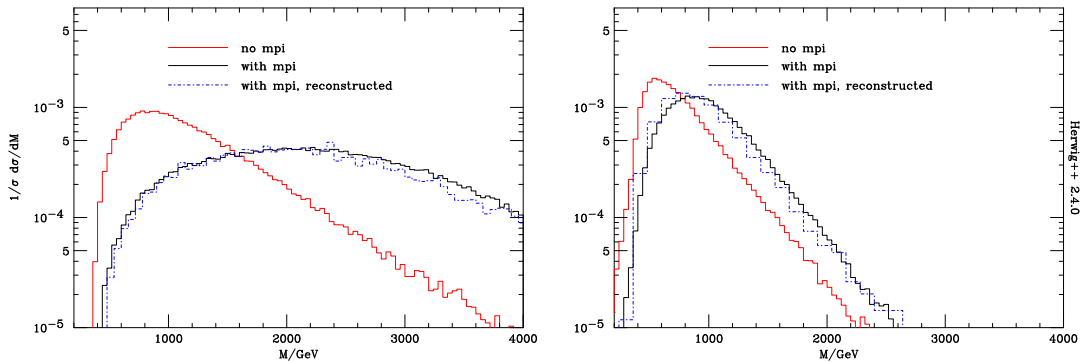


**Figure 12:** The $t\bar{t}$ fully hadronic visible mass distributions for pseudorapity cuts $\eta_{max} = 5$ (left) and $\eta_{max} = 3$ (right), with and without multiple parton interactions (black and red respectively) and the reconstructed curves (blue dot dashes). The $\eta_{\max} = 5$ curve was reconstructed using the resummed results for the visible mass and rapidity, whereas the $\eta_{\max} = 3$ curve was reconstructed using the Monte Carlo visible mass and rapidity.
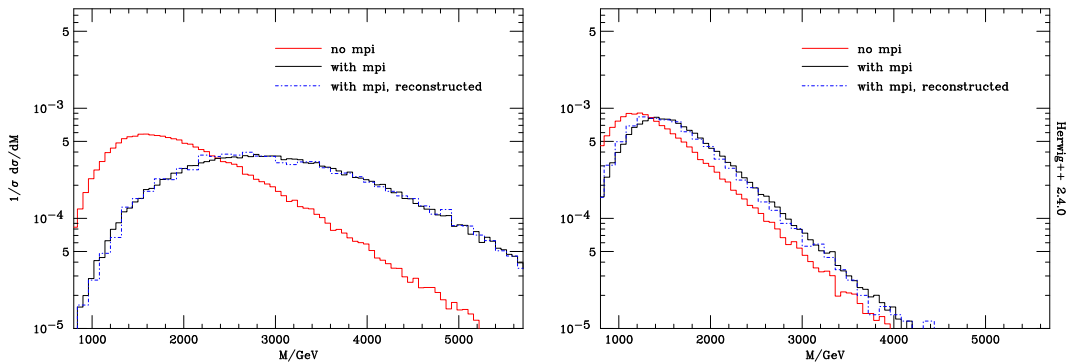
**Figure 13:** The SPS1a gluino pair-production (with $m_{\tilde{g}} = 604.5$ GeV) visible mass distributions for pseudorapity cuts $\eta_{max} = 5$ (left) and $\eta_{max} = 3$ (right), with and without multiple parton interactions (black and red respectively) and the reconstructed curves from the Monte Carlo visible masses and rapidities (blue dot dashes).

by the convolution procedure outlined above, as shown by the blue dot-dashed curves in Figs. 12 and 13. These features of the underlying event will need to be validated by LHC data on a variety of processes. Accurate modelling of the underlying event is important for practically all aspects of hadron collider physics.

## 5. Conclusions

In this paper we have presented detailed predictions on the total invariant mass $M$ of the final-state particles registered in a detector, as a function of its pseudorapidity coverage $\eta_{\mathrm{max}}$. This quantity provides the dominant contribution to many global inclusive observables such as the new variable $\hat{s}_{\mathrm{min}}^{1/2}$ in (1.2), which can provide information on the energy scales of hard processes. We have extended the resummation method presented in [1] to include the effects of invisible particle emission from the hard process. We have considered the case of one or two invisible particles and presented results for Standard Model top quark pair production and SPS1a gluino pair production, obtained using a numerical Mellin moment inversion method.

In the case of $t\bar{t}$ production the invisible particles are neutrinos from W-boson decays and their effect on the visible invariant mass distribution is small, even when both decays are leptonic. This is mainly a consequence of the small W-boson mass compared to the overall invariant mass, rather than the negligible neutrino mass. For gluino pair production the invisibles are a pair of massive LSPs from squark decays. The LSP mass is again small compared to the overall invariant mass, but the squark masses are not, leading to a substantial downward shift in the visible mass distribution, of the order of the squark mass. In both cases the resummed predictions are in fair agreement with Monte Carlo estimates of the position of the peak in the distribution, provided the pseudorapidity range covered by the detector is large

enough ($\eta_{\max} \gtrsim 3$). For $\eta_{\max} \sim 3$, the difference between the Monte Carlo prediction and resummed predictions is of the order of 100 GeV for both the heavy and light gluino SPS1a points. The agreement becomes worse when the pseudorapidity range is restricted, due to particle loss from the hard process. Table 2 shows the positions of the peaks of the distributions for the Monte Carlo results from `Herwig++` and the resummation.

These comparisons were made with Monte Carlo visible mass distributions at parton level. We found that non-perturbative effects, especially the underlying event, tend to shift the invariant mass distributions to significantly higher values than expected from a purely perturbative calculation. According to the underlying event model used in `Herwig++`, the shift amounts to about 250 GeV at $\eta_{max} = 3$ and 1.2 TeV at $\eta_{max} = 5$. This effect is also expected in other observables sensitive to longitudinal momentum components, such as $\hat{s}_{\min}^{1/2}$. However, in this model the underlying event is only weakly correlated with the rest of the event and hence its effects can be determined once and for all at each collider energy. The modelling of the underlying event is an important feature of the Monte Carlos that needs to be validated by comparison with experiment. Once this has been done, a wide range of global inclusive observables, including the visible invariant mass, will be reliably predicted and useful for establishing the scales of contributing hard subprocesses.

## Acknowledgements

## A. Calculation of the evolution kernels

The evolution kernels, $K_{a'a}(z)$, were calculated using the Mellin inverse transform method. Recall that the Mellin transform is defined by the expression

$$K_N^{b'b} = \int_0^1 dz \, z^{N-1} K_{b'b}(z) \tag{A.1}$$

with inverse

$$K_{a'a}(z) = \frac{1}{2\pi i} \int_C dN z^{-N} K_N^{a'a} \, , \tag{A.2}$$

where the contour $C$ runs parallel to the imaginary axis and is to the right of all singularities of the integrand.

Taking into account the running of the strong coupling, the Mellin transform of the solution of the evolution equation (2.4) is

$$K_N^{ba} = \left( \left[ \frac{\alpha_S(Q_c)}{\alpha_S(Q)} \right]^{p\Delta_N} \right)_{ba}$$

(A.3)

with $p = 6/(11C_A - 2n_f)$ and

$$(\Delta_N)_{ba} = \frac{\pi}{\alpha_S}(\Gamma_N)_{ba} = \int_0^1 dz\, z^{N-1} P_{ba}(z) \,.$$

(A.4)

When computing this expression we need to take into account the fact that $\Delta_N$ is a matrix. This can be done most easily by writing it as

$$K_N^{a'a} = \left( \mathcal{O}^{-1} \left[ \frac{\alpha_S(Q_c)}{\alpha_S(Q)} \right]^{p\,\mathrm{diag}(\lambda_{N,i})} \mathcal{O} \right)_{a'a} \,,$$

(A.5)

where $\mathcal{O}$ is the matrix of eigenvectors of $\Delta_N$ and $\mathrm{diag}(\lambda_N, i)$ is the diagonal matrix of its eigenvalues. This is equivalent to using, implicitly, the singlet and non-singlet basis for the PDF evolution [7].
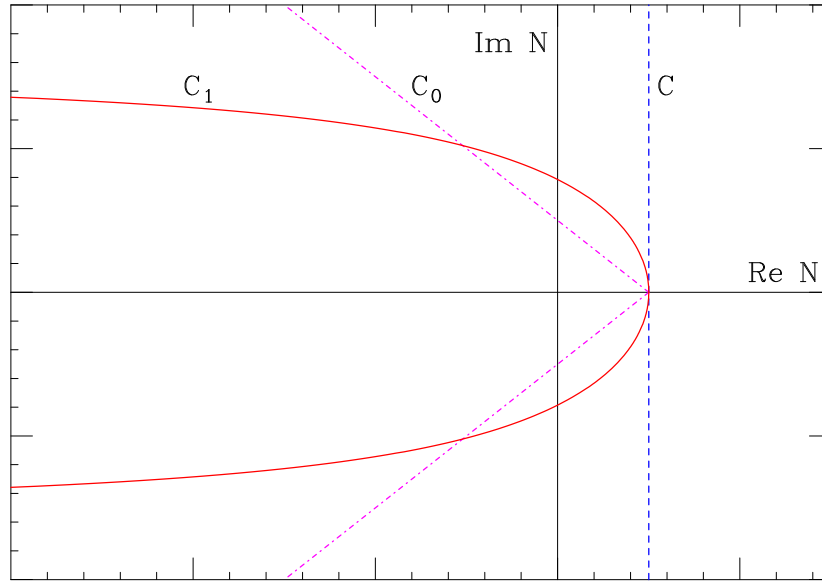


**Figure 14:** Integration contours, $C_0$ and $C_1$, for the inverse Mellin transform as given by the Bromwich integral, eq. (A.2).

To evaluate the inverse transform (A.2), numerical convergence of an otherwise infinitely oscillatory expression is achieved by choosing a contour that introduces a damping factor. A method commonly used in PDF evolution (see, for example, [14]) is to rotate the upper and lower portions of the vertical contour so that they slope

back into the left half-plane, as shown by $C_0$ in Fig. 14. This introduces exponential damping along the contour, which is chosen so as to enclose the same singularities as the 'Bromwich' contour $C$, and therefore converges to the correct result by Cauchy's theorem. However, in the case of the evolution kernels $K_{a'a}(z)$ the linear contour $C_0$ does not provide sufficient accuracy to reproduce the function from its transform. This is due to its inability to invert the constant function $f_N = c$ to the correct analytic result, a delta function. This implies that the inversion does not reproduce the necessary initial condition of the evolution, $K_{a'a}(z, Q = Q_c) \propto \delta(1 - z)$. A numerically more accurate contour is available in the literature, used in the so-called 'Fixed-Talbot algorithm'. This contour $C_1$ has the form $\text{Re}(N) = \text{Im}N \cot(\text{Im}N/r)$ where $r$ is a parameter which we set to $r = 0.4m/\log(1/z)$ during the computation, $m$ being the required precision in number of decimal digits, a value derived from numerical experiments. The contour is related to the steepest descent path for a certain class of functions. For further details on its origin and accuracy see [15].

## B. Pair-production cross sections

The leading-order parton-level cross section for QCD pair-production of particles of mass $m_p$ may be written in terms of scaling functions $f_{ij}$ as

$$\hat{\sigma}_{ij}(Q^2) = \frac{\alpha_S^2(Q^2)}{m_p^2} f_{ij} \ . \tag{B.1}$$

For heavy quark pair-production, the functions for gluon-gluon and quark-antiquark initial states are given by [7]:

$$f_{gg} = \frac{\pi\beta\rho}{27}(2 + \rho) \ , \tag{B.2}$$

$$f_{q\bar{q}} = \frac{\pi\beta\rho}{192}\left[\frac{1}{\beta}(\rho^2 + 16\rho + 16)\log\left(\frac{1+\beta}{1-\beta}\right) - 28 - 31\rho\right] \ . \tag{B.3}$$

where $\rho = 4m_q^2/Q^2$ and $\beta = \sqrt{1-\rho}$. For the case of gluino pair-production, the equivalent functions $f_{ij}$ are given by [16]:

$$f_{gg} = \frac{\pi m_{\tilde{g}}^2}{Q^2}\left\{\left[\frac{9}{4} + \frac{9m_{\tilde{g}}^2}{Q^2} - \frac{9m_{\tilde{g}}^4}{Q^4}\right]\log\left(\frac{1+\beta}{1-\beta}\right) - 3\beta - \frac{51\beta m_{\tilde{g}}^2}{4Q^2}\right\} \ , \tag{B.4}$$

$$\begin{aligned}
f_{q\bar{q}} = \frac{\pi m_{\tilde{g}}^2}{Q^2}\Bigg\{&\beta\left[\frac{20}{27} + \frac{16m_{\tilde{g}}^2}{9Q^2} - \frac{8m_-^2}{3Q^2} + \frac{32m_-^4}{27(m_-^4 + m_{\tilde{q}}^2 Q^2)}\right] \\
&+ \left[\frac{64m_{\tilde{q}}^2}{27Q^2} + \frac{8m_-^4}{3Q^4} - \frac{16m_{\tilde{g}}^2 m_-^2}{27Q^2(Q^2 - 2m_-^2)}\right]\log\left(\frac{1 - \beta - 2m_-^2/Q^2}{1 + \beta - 2m_-^2/Q^2}\right)\Bigg\} \ ,
\end{aligned} \tag{B.5}$$

where now $\beta = \sqrt{1 - 4m_{\tilde{g}}^2/Q^2}$ and $m_-^2$ represents the mass-squared difference between the gluino and the t-channel squark, $m_-^2 = m_{\tilde{g}}^2 - m_{\tilde{q}}^2$.

# References

[1] A. Papaefstathiou and B. Webber, "Effects of QCD radiation on inclusive variables for determining the scale of new physics at hadron colliders," *JHEP* **06** (2009) 069, 0903.2013.

[2] P. Konar, K. Kong, and K. T. Matchev, "$\sqrt{\hat{s}}_{min}$ : A Global inclusive variable for determining the mass scale of new physics in events with missing energy at hadron colliders," *JHEP* **03** (2009) 085, 0812.1042.

[3] M. Bahr *et al.*, "Herwig++ Physics and Manual," *Eur. Phys. J.* **C58** (2008) 639–707, 0803.0883.

[4] R. Brent, *Algorithms for Minimization without Derivatives*. NJ: Prentice-Hall, 1973.

[5] M. Galassi, K. Davies, J. Theiler, J. Gough, G. Jungman, P. Alken, M. Booth, and F. Rossi, *GNU Scientific Library Reference Manual (3rd Ed.)*. Network Theory Ltd, 2009.

[6] F. Hubaut, E. Monnier, P. Pralavorio, K. Smolek, and V. Simak, "ATLAS sensitivity to top quark and $W$ boson polarization in $t\bar{t}$ events," *Eur. Phys. J.* **C44S2** (2005) 13–33, hep-ex/0508061.

[7] R. Ellis, W. Stirling, and B. Webber, *QCD and Collider Physics*. Cambridge University Press, 1996.

[8] **The ATLAS** Collaboration, G. Aad *et al.*, "Expected Performance of the ATLAS Experiment - Detector, Trigger and Physics," 0901.0512.

[9] A. Sherstnev and R. S. Thorne, "Parton Distributions for LO Generators," *Eur. Phys. J.* **C55** (2008) 553–575, 0711.2473.

[10] A. Sherstnev and R. S. Thorne, "Different PDF approximations useful for LO Monte Carlo generators," 0807.2132.

[11] B. C. Allanach *et al.*, "The Snowmass points and slopes: Benchmarks for SUSY searches," *Eur. Phys. J.* **C25** (2002) 113–123, hep-ph/0202233.

[12] B. R. Webber, "A QCD Model for Jet Fragmentation Including Soft Gluon Interference," *Nucl. Phys.* **B238** (1984) 492.

[13] J. M. Butterworth, J. R. Forshaw, and M. H. Seymour, "Multiparton interactions in photoproduction at HERA," *Z. Phys.* **C72** (1996) 637–646, hep-ph/9601371.

[14] A. Vogt, "Efficient evolution of unpolarized and polarized parton distributions with QCD-PEGASUS," *Comput. Phys. Commun.* **170** (2005) 65–92, hep-ph/0408244.

[15] J. Abate and P. Valkó, "Multi-precision Laplace transform inversion," *International Journal for Numerical Methods in Engineering* **60** (2004) 979–993.

[16] W. Beenakker, R. Hopker, M. Spira, and P. M. Zerwas, "Gluino pair production at the Tevatron," *Z. Phys.* **C69** (1995) 163–166, `hep-ph/9505416`.